ANALYSIS OF INFLOW CONDITION EFFECTS ON THE SHEAR LAYER CHARACTERISTICS OF A SUBSONIC JET

Carlos A. S. Moser, carlos.moser@yahoo.com.br
Marcello A. F. Medeiros, marcello@sc.usp.br
University of São Paulo, Av. Trabalhador São-Carlense 400, São Carlos SP 13566-590

Jorge H. Silvestrini, jorgehs@pucrs.br
Pontifícia Universidade Católica do Rio Grande do Sul, Av. Ipiranga 6681, Porto Alegre RS, 90169-900

Abstract. *Effects of the inflow conditions on the shear layer characteristics of a subsonic jet at high Reynolds number were investigated by an implicit large-eddy simulation method. Unlike Smagorinsky eddy-viscosity type methods, this approach assumes that the subgrid-scale model may be determined by the structure of the resolved flow and, therefore, does not require the addition of subgrid-scale stress or heat flux terms to the flow governing equations. In order to accurately solve the large difference of scales between the aerodynamic and acoustic field, high-order compact finite difference schemes were used for spatial discretization and a fourth-order Runge-Kutta method was employed for time integration. The high-frequency content of the smallest unresolved subgrid scales was removed by the application of high-order compact filtering, while the effect of the smallest unresolved scales on the filtered scales was reconstructed by an approximate deconvolution model. The non-conservative form of the fully compressible Navier-Stokes equations was used to compute the flow solution in the physical domain and a characteristic-based formulation was used to prescribe boundary conditions and buffer zone treatments especially adapted for aeroacoustic computations. Inflow conditions effects on the jet shear-layer characteristics, such as the jet inlet momentum tickness, were analysed in the well-known test case of a Mach* 0.9 *jet at Reynolds number* 6.5×10^4*. The present results were found to be in good agreement with previous numerical results found in the literature at the same flow conditions. In the ongoing work, a parallel high-order flow solver is being implemented to perform the implicit large-eddy simulation of noise radiated by subsonic three-dimensional round jets at high Reynolds number.*

Keywords: *Computational aeroacoustics, subsonic jet, implicit large-eddy simulation, high-order methods.*

1. INTRODUCTION

In traditional large-eddy simulation (LES) methods, the governing equations are obtained by the spatial filtering of the flow variables. Ideally, for incompressible flows the filtering of the Navier-Stokes equations generates a closure problem in the form of an unknown residual subgrid-scale stress tensor:

$$\tau_{i,j} = \overline{u_i u}_j - \bar{u}_i \bar{u}_j \tag{1}$$

The filtering equations are not closed because of the presence of the nonlinear term $\overline{u_i u}_j$. It should be emphasized, however, that the subgrid-scale stress tensor stems from a closure problem introduced by the spatial filtering operation and not from the discretization's inability to represent the small scales in the flow. As a result, the subgrid-scale stress tensor strongly depends on the assumed filter shape, which causes a subgrid-scale model to be inherently filter dependent. Hence, depending on the choice of the filter, the corresponding model should satisfy very different requirements in terms of large-scale dynamics and kinetic energy budget.

The subgrid-scale Smagorinsky eddy-viscosity type models widely used today for LES of compressible flows remain at best semiempirical, since they require tuning of modeling coefficients to obtain reliable noise predictions. These models exhibit two major drawbacks. They ignore turbulence anisotropy and use a local balance assumption between the subgrid scale turbulence kinetic energy production and its dissipation. Furthermore, they predict non-vanishing subgrid eddy viscosity in regions where the flow is laminar. The dynamic procedures (Germano, Piomelli and Moin, 1991, Lilly, 1992) for computing the model coefficient from the resolved velocity field, which require no adjustable constant, overcome these shortcomings. However, the numerical stabilization become complicated when the dynamic model is applied to flow configurations in which there are inhomogeneous directions. Vreman (2004a) developed a subgrid eddy-viscosity type model especially suitable for laminar shear flows, since it vanishes subgrid dissipation in laminar regions and does not require any averaging or clipping procedure for numerical stabilization. Park, Lee and Choi (2006) proposed a dynamic procedure for determining the model coefficient utilizing the global equilibrium between the subgrid and viscous dissipation. In this approach, the model coefficient is globally constant in space but varies in time, and it still garantees zero eddy viscosity in the laminar regions of the flow.

2. NUMERICAL METHOD

As an alternative approach to subgrid-scale Smagorinsky eddy-viscosity type models we use high-order spatial filters to implictly model the energy content present in the poorly resolved smallest scales of the flow. This aproach does not require any additional subgrid scale stress or heat flux terms in the flow governing equations. Although the filter is applied explicitly to the evolving solution, this approach is referred as implicit LES, since the application of the spatial filter is a fundamental component to mantain stability by removing high-frequency spurious numerical oscillations. The basis of the implicit LES approach is that the numerical truncation error associated with the discretization has similar form or action to the subgrid model. Such approach falls into the class of structural models, since there is no assumed form of the nature of the subgrid flow. The subgrid model is entirely determined by the structure of the resolved flow (Sagaut, 2001). Nevertheless, even with the recently increase of interest in implicit LES, there is not a consensus on the appropriate form of the discretization error, since it is assumed that the numerics provide sufficient modeling of the subgrid terms to allow correct dissipation of turbulent kinetic energy.

The analysis of the impact of spatial discretization errors on implicit LES establishes the need of high-order spatial filtering (Gaitonde and Visbal, 1999). The high order filtering of Navier-Stokes equations should provides dissipation at the higher modified wave numbers only, where the spatial discretization already exhibits significant dispersion errors, and enforce numerical stability on nonuniform grids. The filtering also should allow to eliminate numerical instabilities arising from poor grid quality, unresolved scales, or boundary conditions, which left to grow can potentially corrupt the flow solution. The filtering operation is defined by Leonard (1974) in the physical space as

$$\bar{f}(x) = \int_{\Omega} f(x')G(x,x';\delta)dx' \tag{2}$$

where Ω is the entire domain, G is the filter kernel and δ is the filter width associated to the smallest scale retained by the filtering operation. Thus, $\bar{f}$ defines the size and structure of the small scales.

In principle, to mantain acceptable numerical acurracy and proper resolution of low wavenumbers, the filter accuracy should be equal or greater than the corresponding accuracy of the spatial discretization scheme. Thus, in this work the flow variables were filtered in every spatial direction at the final stage of each time step with sixth-order implicit filters (Visbal and Gaitonde, 2001). Sixth-order compact finite difference schemes (Lele, 1992) were employed for the spatial discretization and the fourth-order Runge-Kutta method was used for the temporal integration.

At the interior grid points $i = 4, ..., N-3$, the implicit filtering approach is defined as follows

$$\alpha_f \bar{f}_{i-1} + \bar{f}_i + \alpha_f \bar{f}_{i+1} = \sum_{n=1}^{4} \frac{a_n}{2}(f_{i-n+1} + f_{i+n-1}) \tag{3}$$

The coefficients a_n are derived in terms of the filtering parameter α_f by Taylor and Fourier series analysis (Gaitonde and Visbal, 1998, 1999), where α_f must satisfy the inequality $-0.5 \leq \alpha_f \leq 0.5$. Filters less dissipative are obtained with higher values of α_f within the given range, and for $\alpha_f = 0.5$ there is no filtering effect. By contrast, the explicit filter ($\alpha_f = 0$) display significant degradation of the spectral frequency response. Here α_f was fixed as 0.40.

As equation (3) has a right-hand side stencil of seven points, obviously it can not be employed near the boundaries of the computational domain. Thus, the following implicit filter is used at the grid points $i = 2$ and 3:

$$\alpha_f \bar{f}_{i-1} + \bar{f}_i + \alpha_f \bar{f}_{i+1} = \sum_{n=1}^{7} a_{n,i} f_n, \tag{4}$$

and analogously, at the grid points $i = N-2$ and $N-1$, while at the boundary points $i = 1$ and N, the flow variables were kept without application of any filtering operation.

In the present study, the implicit LES approach re-interpreted by Mathews et al. (2003) in the context of an approximate deconvolution model (Stolz and Adams, 1999) was employed to compute the filtered solution variable $\bar{u}$, by the following filtering operation

$$\bar{u} = G * u = \int G(x - x')u(x')dx' \tag{5}$$

where G is the filter transfer function. If G has an inverse Q, an approximation of the unfiltered variable u, denoted by u^*, may be obtained by deconvolution of the filtered variable $\bar{u}$ as

$$u^* = Q * \bar{u} \tag{6}$$

where the inverse filter transfer function Q may be obtained by a truncated power series expansion

$$Q_N = \sum_{\nu=0}^{N} (I - G)^{\nu} \tag{7}$$

where I is the identity matrix and $N = 1, 2, 3, ...$ the number of filtering steps. The family of inverse filter transfer functions, Q_N, is based on the iterative deconvolution method of Galdi (2000). High-order approximations u^* from the unfiltered variable u, can be derived by sucessive filtering operations applied to the filtered quantities

$$u^* = \bar{u} + (I - G) * \bar{u} + (I - G) * ((I - G) * \bar{u}) + ... \tag{8}$$

In smooth regions of the flow, these filters have strong stability properties and high-order consistency error $O(\delta^{2N+2})$, where δ is the filter width. As reported by Stolz, Adams and Kleiser (2001a), the truncation order of the Eq. (8) determines the level of deconvolution. Here we choose the third level quadratic extrapolation: $u^* \approx Q_2\bar{u} := 3\bar{u} - 3\bar{\bar{u}} + \bar{\bar{\bar{u}}}$, since it affords a sufficiently high-order consistency error $O(\delta^5)$.

3. FLOW CONFIGURATION

In this work, the jet nozzle exit has been modeled by imposing at the inflow boundary the following hyperbolic-tangent mean velocity profile

$$u(r) = \frac{U_j}{2}\left(1 + \tanh\left(\frac{r_o - r}{2\delta_\theta}\right)\right) \tag{9}$$

where U_j is the jet inlet centerline velocity, r_o is the jet radius and δ_θ is the inlet shear-layer momentum thickness.

The jet inlet velocities were normalized by the sound speed in the ambient medium c_o. The Mach number of the flow was set to 0.9 and the Reynolds number to $Re_D = U_j\, D/\nu = 6.5 \times 10^4$, with $D = 2r_o$ the jet width and ν the kinematic viscosity. The choice of this Mach number may be justified by the considerable amount of numerical and experimental studies at similar flow conditions. The Reynolds number adopted is an intermediate value between jets obtained by DNS ($Re_D < 10^3$) and experimental jets ($Re_D > 10^5$). The inlet momentum thickness was chosen as $\delta_\theta = 0.05r_o$, which is large enough to afford the development of turbulent structures in the jet shear layer before the end of the potential core.

In order to reduce the inherently high computational cost of 3D computations, the preliminary tests for evaluation and validation of the present implicit LES approach were performed in a two-dimensional domain. As show Fig.1, the mesh was discretized in Cartesian coordinates with 255×225 grid points in a computational domain which extends to $50r_o$ in the streamwise direction and from $-25r_o$ to $25r_o$ in the transverse direction. As the velocity gradients are more pronounced in the jet shear layer, the mesh was more refined in this region, with an uniform grid spacing of $\Delta y = r_o/32$. Outside the shear layer the grid was gradually stretched up to an uniform grid spacing of $0.602r_o$ in the acoustic field. In the streamwise direction, the grid discretization was relatively coarser, with an uniform grid spacing of $0.071r_o$ from the jet inlet up to the end of the potential core. The grid was gradually stretched downstream of the potential core up to a maximum grid spacing of $1.402r_o$ at the outflow boundary.

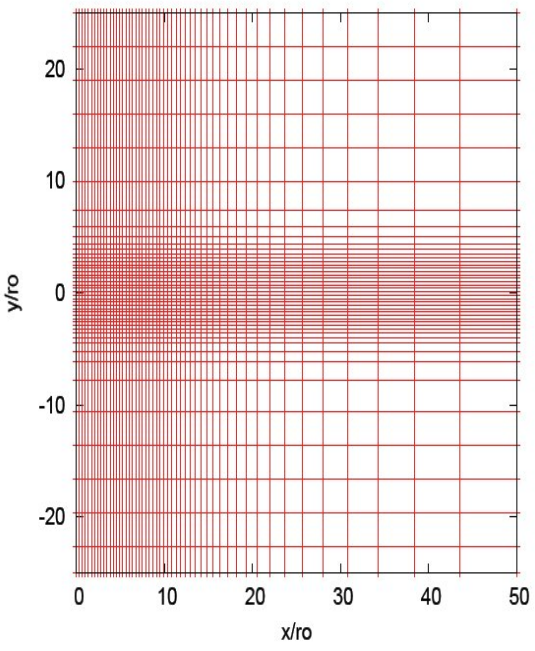

Figure 1. Mesh discretization in the computational domain. Representation of one grid point over five in both directions.

3.1 Near-inlet disturbance

In order to startup earlier the transition to the turbulent mixing process in the jet shear layer, a low-amplitude disturbance of incompressible nature (Bogey and Bailly, 2005a) is superimposed onto the base flow velocity profile (9), just downstream of the inflow boundary. The jet shear layer instabilities are governed by two different modes associated with two different characteristic length scales: the inlet shear-layer momentum thickness δ_θ and the jet width D. The first mode is the fundamental frequency f_o of the velocity fluctuations. This mode is observed in the neighborhood of the jet inlet and is responsible by the exponential growth of shear layer instabilities. The linear instability theory (Michalke, 1964) predicts that the strongest amplification rate of disturbances for the hyperbolic-tangent velocity profile given by Eq. (9) is observed for $fo = 0.017U_j/\delta_\theta$. The second mode, known as the first sub-harmonic $f_1 = f_o/2$, corresponds to the frequency of the vortex pairing process. In the current calculations this mode also characterizes the frequency of the velocity fluctuations that occurs in the jet potential core, with amplitudes fixed as $\alpha_o = 2.5 \times 10^{-4}$ and $\alpha_1 = \alpha_o/3$.

3.2 Non-reflecting boundary conditions and buffer zone treatments

In the present computations, the domain considered is large enough to allow acoustic wave propagation in the far-field. Thus, far-field non-reflecting boundary conditions were obtained by simply setting to zero the incoming waves at the outflow and lateral boundaries. Reflections of spurious waves generated at the inflow boundary by the near-inlet disturbance were minimized by the application of a near-inflow acoustic absorbing zone (Moser, Lamballais and Gervais, 2006).

Similarly to Colonius, Lele and Moin (1993), a buffer zone of aerodynamic dissipation was attached downstream of the physical domain to damp large-scale vortical structures originated by the turbulent jet flow. These structures are effectively dissipated in the buffer zone, before they interact with the outflow boundary, by superimposing artificial damping terms to the flow governing equations

$$\left.\frac{\partial \mathbf{Q}}{\partial t}\right|_{dp} = \frac{\partial \mathbf{Q}}{\partial t} - \sigma_{dp}\mathbf{Q}' \tag{10}$$

$\mathbf{Q}$ is the solution vector $[u, p]$ and σ_{dp} is a damping function defined as

$$\sigma_{dp}(r) = \frac{1}{4}\left(1 + \tanh\left(a_o \frac{r - 2r_o}{2\delta_\theta}\right)\right) \tag{11}$$

with $r^2 = x^2 + y^2$ and $a_o = 0.575$.
The disturbance $\mathbf{Q}'$ in the Eq. (10) is computed at every time step t as follows

$$\mathbf{Q}'_{(t)} = \mathbf{Q}_{(t)} - \left(\alpha \bar{\mathbf{Q}}_{(t-1)} + (1-\alpha)\mathbf{Q}_{(t)}\right) \tag{12}$$

where $\bar{\mathbf{Q}}_{(t-1)}$ is the time-average solution computed in the previous time step and $\alpha = 0.90$. Additionally, was applied in the buffer zone the grid stretching to help to dissipate the large-scale disturbances of the jet flowfield.

4. RESULTS

As reported by several studies of jets (Bradshaw, 1966, Hill, Jenkins and Gilbert, 1976, Keiderling, Kleiser and Bogey, 2009) the development of turbulence by the jet is very sensitive to small variations on the inflow conditions characterizing the jet shear layer evolution. Kim and Choi (2009) observed that inflow conditions effects on jet characteristics, as the inlet momentum thickness and the Reynolds number, substantially depend on the accurate resolution of the jet shear layer. In the LES of a 3D round jet Bogey (2000) employed 26 grid points to discretize the jet half-width. However, the LES of round jets using explicit selective/high-order filtering (Bogey and Bailly, 2006) the jet radius was discretized in a Cartesian grid with 15 points. Therefore, understanding grid resolution effects on the jet characteristics may be critical for predicting the jet flow dynamics.

4.1 Grid resolution effects on the jet shear layer characteristics

The effects of grid resolution were investigated by forcing the near-inlet shear layer region, just downstream of the inflow boundary, with low-amplitude periodic and random disturbances. The inverse of the jet mean centerline velocity, U_c, normalized by the jet inlet mean centerline velocity, U_j, is represented in Fig.2 for different grid resolutions. The grid points were gradually clustered, by locally decreasing the grid spacing from $\Delta y = r_o/18$ to $r_o/36$ to accurately resolve the large gradients of velocity in the shear layer. When the grid spacing was decreased from $\Delta y = r_o/32$ to $r_o/36$ in the jet shear layer, it may be observed the convergence, since the curves U_j/U_c tend to be superposed. As the initial shear layer evolution is laminar for the current jet inflow conditions ($Re_D = 6.5 \times 10^4$ and $\delta_\theta = 0.05r_o$), it appears that the

jet mean centerline velocity should be constant in the whole jet potential core. However, small fluctuations on the jet mean centerline velocity were detected within the jet potential core, for $5 \leq x/r_o \leq 9$. It is important to notice, that this behavior within the potential core has already been observed experimentally (Islam, 1997) and numerically (Bogey, 2006). In the far downstream region, as expected, we see that the inverse of the jet centerline velocity decaying rate presents linear growth for both periodic and random disturbances. Nevertheless, when the jet near-inlet shear layer region was periodically excited, the potential core breaks up earlier and the inverse of the velocity decaying rate presents smaller growth in the far downstream region.

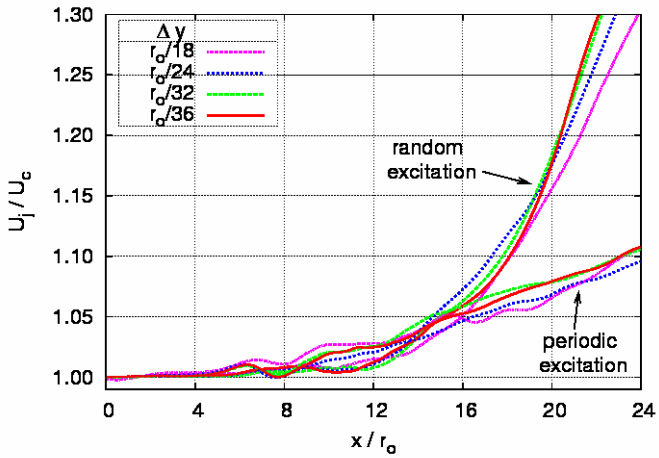

Figure 2. Representation of the inverse of the jet mean centerline velocity, U_c, normalized by the jet inlet mean centerline velocity, U_j, for different grid resolutions in the jet shear layer, excited with random and periodic disturbances.

In figures 3(a)-(d) were evaluated, for different grid resolutions in the jet shear layer, the instantaneous of vorticity field, $\omega_{xy} = \partial v/\partial x - \partial u/\partial y$, of a periodically excited jet. As show Figs.3(a) and (b), for about $x = 3r_o$, the initial shear-layer tickness was strongly affected by the coarser resolutions in the jet shear layer. The coarser meshes introduce an upstream effect on the initial shear layer evolution, such that the initial shear-layer tickness is affected by feedback effects from the downstream development of the large-scale vortices (Dimotakis, 1976). Nevertheless, when finer meshs were used in Figs.3(c) and (d), the initial shear layer evolution was almost unaffected by feedback effects. Thus, for the present shear-layer tickness, $\delta_\theta = 0.05r_o$, it was required to adopt at most the grid spacing of $\Delta y = r_o/32$ in the jet shear layer to achieve accurate predictions of the jet flow dynamics.

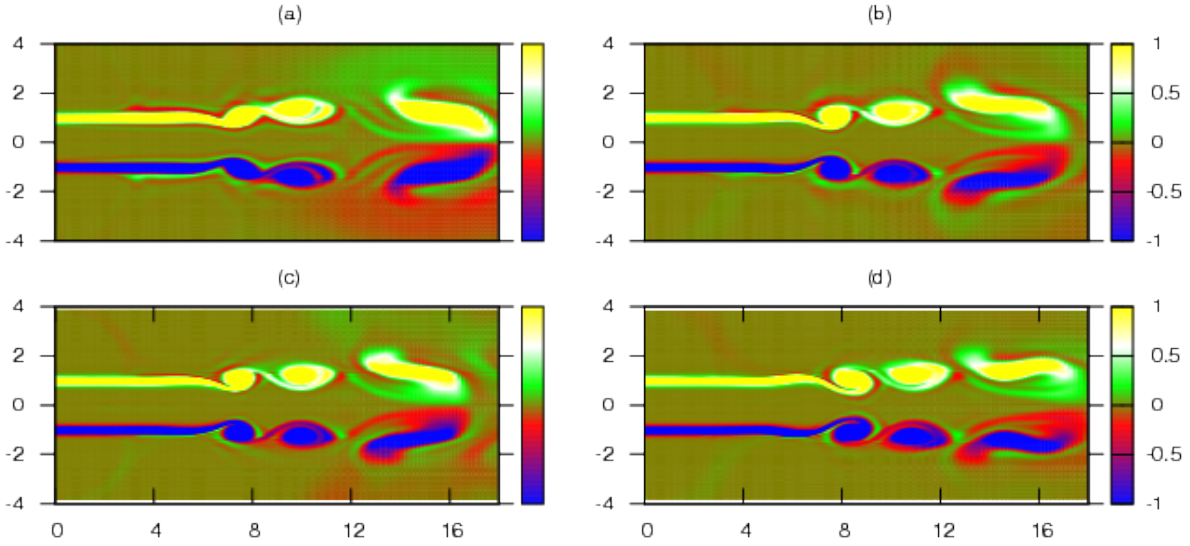

Figure 3. Representation of the vorticity field, ω_{xy}, for the grid resolutions: (a) $\Delta y = r_o/18$; (b) $r_o/24$; (c) $r_o/32$ and (d) $r_o/36$ in the jet shear layer. Physical domain for $0 \leq x/r_o \leq 18$ and $-4 \leq y/r_o \leq 4$.

4.2 Aerodynamic flow noise-source and acoustic field propagation

The aerodynamic flow noise-source region and the acoustic field propagation are represented in Fig.4 by the vorticity, ω_{xy}, and dilatation, Θ. It is important to remark that both fields were directly computed by the present implicit LES procedure without the need of any modeling approach. It should be noticed in Fig.4 that the acoustic wavefronts propagate from the region of the aerodynamic field that give rise to the vortex pairing process, which is located at the end of the potential core at around $x/r_o = 12$. Thus, the only dominant noise source in the jet shear layer is the noise radiated from the region where the vortex pairing takes place. The absence of spurious waves near the inflow is due to the incompressible nature (Bogey, 2005) of the disturbance. It should be noted that the acoustic waves propagate through the far-field boundary without producing any significant spurious wave reflections, because of the application of the nonreflecting boundary condition. The noise radiated on the acoustic field decays to zero for an angle around 80^o, with phase shifting for wider angles of radiation relative to the shear layer axis. This particularly high directive character of sound radiation, especially noticed at high Mach numbers, is attributed to the axisymmetric quadrupolar nature of the sound source, as already observed by LES of three-dimensional jets (Bogey, 2003a).

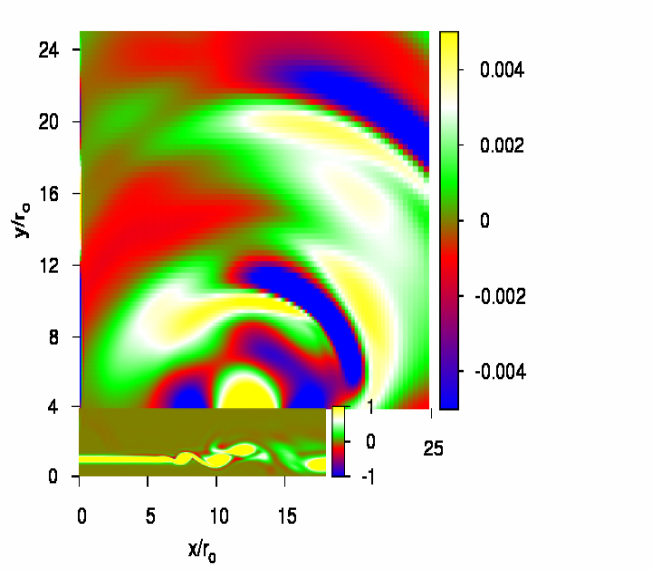

Figure 4. Aerodynamic and acoustic fields represented, respectively, by the vorticity, ω_{xy} and dilatation, Θ. Upper regions of the physical domain, excluding the buffer zone of aerodynamic dissipation located after $x/r_o = 18$.

5. CONCLUDING REMARKS

Preliminary tests were carried out for evaluation and validation of a highly accurate implicit LES approach especially developed for the computation of the aerodynamic noise radiated from a Mach 0.9 cold jet at Reynolds number 6.5×10^4. In order to startup earlier the transition to the turbulent mixing process in the jet shear layer, the near-inlet shear layer region was forced with low-amplitude periodic or random disturbances. Effects of grid resolution on the jet shear layer characteristics were investigated for the jet inlet shear layer momentum thickness $\delta_\theta = 0.05 r_o$. The evaluation of the vorticity field, ω_{xy}, for different grid resolutions, shows that the initial shear layer tickness was strongly affected by the coarser grid resolutions. In fact, a maximum grid spacing in the jet shear layer of $\Delta y = r_o/32$ was required for the accurate prediction of the jet flow dynamics. It was observed that the introduction of a near-inflow periodic disturbance trigger the growth of Kelvin-Helmholtz instabilities, which rapidly evolve downstream to give rise to the vortex pairing process in the jet shear layer. The aerodynamic development of the vortex pairing proccess presents qualitative agreement with previous results taken from the literature (Bogey, 2000) at the same flow conditions (Reynolds number, Mach number and jet inlet momentum thickness). The analysis of the corresponding acoustic field propagation shows that the dominant sound source produced in the jet shear layer was the sound radiated from the vortex pairing process, without any significant wave oscillations provided by the disturbance. The particularly high directive character of sound radiation, especially noticed at high Mach numbers, was attributed to the axisymmetric quadrupolar nature of the noise source. In the ongoing works, a parallel high-order finite-sized overlap flow solver is being developed to investigate Mach number and thermal instability effects arising from three-dimensional round jets. It is hoped that high Reynolds number 3D computations of both cold and heated jet flow-noise sources and its inherently coupled noise propagation will allow us to investigate more deeply the underlying nonlinear mechanisms by which noise is aerodynamically generated in turbulent free shear layer flows at less idealized flow conditions.

6. ACKNOWLEDGEMENTS

This research project in computational aeroacoustics was supported by the Laboratory of Aerodynamics of the Department of Aeronautical Engineering, University of São Paulo, Brazil. The project was sponsered by FAPESP (Fundação de Amparo à Pesquisa do Estado de São Paulo) which we gratefully thank for the financial support.

7. REFERENCES

Bogey, C., 2000, "Calcul direct du bruit aérodynamique et validation de modèles acoustiques hybrides", Thesis, École Centrale de Lyon, Lyon - France.

Bogey, C., Bailly, C. and Juvé, D., 2003a, "Noise investigation of a high subsonic, moderate Reynolds number jet using a compressible large eddy simulation", Vol. 16, No. 4, pp. 273-297.

Bogey, C. and Bailly, C., 2005a, "Effects of inflow conditions and forcing on subsonic jet flows and noise", AIAA J..

Bogey, C. and Bailly, C., 2006, "Computation of a high Reynolds number jet and its radiated noise using large eddy simulation based on explicit filtering", Computat. Fluids, Vol. 33, pp. 1344-1358.

Bradshaw, P., 1966, "The effect of initial conditions on the development of a free shear layer", J. Fluid Mech..

Colonius, T., Lele, S. K. and Moin P., 1993, "Boundary condition for direct computation of aerodynamic sound generation".

Dimotakis, P. E. and Brown, G. L., 1976, "The mixing layer at high Reynolds number: Large-structure dynamics and entrainment", J. Fluid Mech., Vol. 78, pp. 535-560.

Gaitonde, D. V. and Visbal, M. R., 1998, "High-order schemes for Navier-Stokes equations. Algorithm and implementation into FDL3DI",Technical Report AFRLVA-WP-TR-1998-3060, Air Force Research Laboratory, Wright-Patterson, AFB.

Gaitonde, D. V. and Visbal, M. R., 1999, "Further Development of a Navier-Stokes Solution Procedure Based on Higher-Order Formulas", AIAA Paper No. 99-0557.

Galdi, G. P., 2000, Lectures in Mathematical Fluid Dynamics, Birkhäuser-Verlag, Basel, Switzerland.

Germano, M., Piomelli, U. and Moin, P.,1991,"A dynamic subgrid-scale eddy viscosity model", Phys. Fluids,Vol.3, pp. 1760-1765.

Hill, Jr. W., Jenkins, R. C. and Gilbert, B. L., 1976, "Effects of the initial boundary-layer state on turbulent jet mixing", AIAA J., Vol. 14, pp. 1513-1514.

Islam, M. T. and Ali, M. A. T., 1997, "Mean velocity and static pressure distributions of a circular jet", AIAA J, Vol. 35, pp. 196-197.

Keiderling, Kleiser and Bogey, 2009, "Numerical study of eigenmode forcing effects on jet flow development and noise generation mechanisms", Phys. Fluids, Vol. 21, 045106.

Kim, J. and Choi, H., 2009, "Large eddy simulation of a circular jet: effect of inflow conditions on the near field", J. Fluid Mech., Vol. 620, pp. 383-411.

Lele, S. K., 1992, "Compact finite difference schemes with spectral like resolution", J. Comput. Phys., Vol. 103, pp. 16-42.

Lilly, D., 1992, "A proposed modication of Germano subgrid-scale closure method", Phys. Fluids, Vol.4, pp. 633-635.

Mathews, J., Lechner, R., Foysi, H., Sesterhenn, J. and Friedrich, R., 2003, "An explicit filtering method for large eddy simulation of compressible flow", Phys. Fluids, Vol. 15, No. 8, pp. 2279-2289.

Michalke, A., 1964, "On the inviscid instability of the hyperbolic-tangent velocity prole", J. Fluid Mech., Vol. 19, pp. 543-566.

Moser, C. and Lamballais, E. and Gervais, Y., 2006, "Direct computation of the sound generated by isothermal and non-isothermal mixing layers", The 12th AIAA/CEAS Aeroacoustic conference, AIAA 2006-2447.

Park, N., Lee, S. and Choi, H., 2006, "A dynamic subgrid-scale eddy-viscosity model with a global model coefficient", Phys. Fluids, Vol. 18, pp. 125-129.

Sagaut, P., 2001, "Large Eddy Simulation for Incompressible Flows", Ed. Springer Verlag.

Stolz, S. and Adams, N.A., 1999, "An approximate deconvolution procedure for large eddy simulation", Phys. Fluids, Vol. 11, pp. 1699-1701.

Stolz, S., Adams, N.A. and Kleiser, L., 2001a, "An Approximate Deconvolution Model for Large-Eddy Simulations of Compressible Flows and Its Application to Shock-Turbulent-Boundary-Layer Interaction", Phys. Fluids, Vol. 13, pp. 2985-3001.

Visbal, M. R. and Gaitonde, D. V., 2001, "Very high-order spatially implicit schemes for computational acoustics on curvilinear meshes", J. Comput. Acoust., Vol. 9, No. 1, pp. 16-42.

Vreman, A. W., 2004a,"An eddy-viscosity subgrid-scale model for turbulent shear flow: algebraic theory and applications", Phys. Fluids, Vol.16, No. 10, pp. 3670-3681.

8. Responsibility notice

The authors are the only responsible for the printed material included in this paper.